Temperature Dependence of the Internal Dynamics of a Calmodulin−Peptide Complex†

Andrew L. Lee,‡ Kim A. Sharp, James K. Kranz,§ Xiang-Jin Song, and A. Joshua Wand*

The Johnson Research Foundation and Department of Biochemistry and Biophysics, University of Pennsylvania, Philadelphia, Pennsylvania 19104-6059

Received July 1, 2002; Revised Manuscript Received September 10, 2002

ABSTRACT: The temperature dependence of the fast internal dynamics of calcium-saturated calmodulin in complex with a peptide corresponding to the calmodulin-binding domain of the smooth muscle myosin light chain kinase is examined using ^{15}N and ^{2}H NMR relaxation methods. NMR relaxation studies of the complex were carried out at 13 temperatures that span 288−346 K. The dynamics of the backbone and over four dozen methyl-bearing side chains, distributed throughout the calmodulin molecule, were probed. The side chains show a much more variable and often considerably larger response to temperature than the backbone. A significant variation in the temperature dependence of the amplitude of motion of individual side chains is seen. The amplitude of motion of some side chains is essentially temperature-independent while many show a simple roughly linear temperature dependence. In a few cases, angular order increases with temperature, which is interpreted as arising from interactions with neighboring residues. In addition, a number of side chains display a nonlinear temperature dependence. The significance of these and other results is illuminated by several simple interpretative models. Importantly, analysis of these models indicates that changes in generalized order parameters can be robustly related to corresponding changes in residual entropy. A simple cluster model that incorporates features of cooperative or conditional motion reproduces many of the unusual features of the experimentally observed temperature dependence and illustrates that side chain interactions result in a dynamically changing environment that significantly influences the motion of internal side chains. This model also suggests that the intrinsic entropy of interacting clusters of side chains is only modestly reduced from that of independent side chain motion. Finally, estimates of protein heat capacity support the view that the major contribution to the heat capacity of protein solutions largely arises from local bond vibrations and solvent interactions and not from torsional oscillations of side chains.

The physical basis of protein structure, dynamics, and stability continues to be a subject of intense study and discussion. Though the taxonomy of protein structure is becoming well understood, a similar depth of understanding of the existence and character of internal protein motion remains to be achieved. The importance of understanding the nature of protein dynamics is manyfold. For example, in the classical view of the thermodynamics of protein folding and stability, it is argued that the penalty of going from an unfolded state of high entropy to a folded state of low residual entropy is largely overcome by the entropic gain derived from the release of water-solvating hydrophobic groups in the unfolded state. Recent investigations appear to require refinement of this view. The conformational entropy of the unfolded state has recently been reassessed and suggested to be much smaller than previously imagined (*1*−*3*). In addition, the view provided by NMR[1] spectroscopy suggests that the residual entropy of the folded state may be large (*4*, *5*), which further diminishes the entropic penalty that a protein must pay to fold, in effect narrowing the top and broadening the bottom of the energy landscape funnel (*6*). Fundamental questions about the role of protein dynamics in protein function also clearly remain. Though the view of Pauling (*7*) that the catalytic power of an enzyme arises

† Supported by NIH Grants DK 39806 (A.J.W.) and NSF MCB98-08202 (K.A.S.), by equipment grants from the NIH and the ARO, and by NIH postdoctoral fellowships to A.L.L. (GM 18114) and J.K.K. (GM 20206).

* Address correspondence to this author. Telephone: (215) 573-7288. Facsimile: (215) 573-7290. E-mail: wand@mail.med.upenn.edu.

‡ Present address: Division of Medicinal Chemistry and Natural Products, School of Pharmacy, CB#7360, Beard Hall, University of North Carolina, Chapel Hill, NC 27599-7360.

§ Present address: 3-Dimensional Pharmaceuticals, Inc., 665 Stockton Drive, Exton, PA 19341.

[1] Abbreviations: CaM, calcium-saturated recombinant chicken calmodulin; HSQC, heteronuclear single-quantum spectroscopy; I_zC_z, two-spin longitudinal proton and carbon coherence; $I_zC_zD_z$, three-spin longitudinal proton, carbon, and deuterium coherence; $I_zC_zD_y$, three-spin longitudinal proton and carbon coherence with transverse deuterium coherence; NMR, nuclear magnetic resonance; NOE, nuclear Overhauser effect; smMLCKp, peptide corresponding to the smooth muscle myosin light chain kinase calmodulin-binding domain; ppm, parts per million; σ, linear temperature coefficient for a squared generalized order parameter; O^2, squared generalized order parameter; O_{NH}^2, O^2 of an amide N−H bond vector; O_{axis}^2, O^2 of the symmetry axis of a methyl group; S, entropy; T_1, longitudinal or spin−lattice relaxation time constant; T_2, transverse or spin−spin relaxation time constant; τ_m, overall molecular tumbling correlation time; τ_e, effective correlation time for internal motion; TPPI, time-proportional phase incrementation; Tris-HCl, tris(hydroxymethyl)aminomethane hydrochloride.

10.1021/bi026380d CCC: $22.00
Published on Web 10/24/2002

from its greater affinity for the transition state than for the ground state substrate has been well supported and is now a fundamental principle of enzymology, a supplementary view is that enzymes position reactants to allow thermal motions to carry them efficiently along the reaction coordinate (*8*, *9*). Petsko and co-workers have provided strong evidence that protein motion strongly influences catalytic activity in ribonuclease (*10*). Other examples include a role for protein fluctuations in promoting hydrogen tunneling during catalysis by alcohol dehydrogenase (*11*, *12*) and in modulating intraprotein electron transfer (*13*). These observations raise further questions. Are the general thermally activated random motions of the protein harnessed for catalysis or are "special" fluctuations employed? What are the time scales of kinetically relevant motion?

Initial experimental insights into the character of protein internal motion largely employed local optical probes, unresolved hydrogen exchange, and one-dimensional NMR techniques that, though limited, revealed a startling complexity and richness in the internal motion of proteins (*14*−*18*). These views have been increasingly supplemented with both crystallographic (e.g., refs *10* and *19*) and NMR-based insights. Over the past decade NMR spectroscopy has emerged as a powerful tool for the characterization of protein dynamics in a comprehensive site-resolved manner (*20*, *21*). Many ^{15}N relaxation based studies of backbone dynamics have been reported and generally indicate that the main chain largely acts as a rigid scaffold (*20*, *21*). The current view provided by ^{13}C and ^{2}H NMR relaxation methods suggests that protein hydrophobic cores are quite dynamic and, importantly, heterogeneously so (*6*). The handful of studies of the subnanosecond time scale motion of methyl-bearing side chains reveals a remarkably rich range of motional amplitudes (*22*). A recent surprise is the apparent clustering of methyl-bearing side chains into three general classes of dynamical disorder (*22*).

The structural and stereochemical determinants of this rich dynamical behavior are largely unknown. In this regard, the relationships between structure and dynamics could potentially be illuminated by the temperature dependence of the dynamics. Variation of temperature provides, in principle, access to the energetics of the motional modes contributing to the NMR relaxation phenomena. With this in mind, we have undertaken a comprehensive study of the temperature dependence of the fast main chain and methyl-bearing side chain dynamics of calcium-saturated calmodulin (CaM) in complex with a peptide model for the smooth muscle myosin light chain kinase calmodulin-binding domain (smMLCKp). A synoptic analysis of this study has been reported previously and indicated the aforementioned trimodal distribution of angular disorder in calmodulin and that the temperature dependence of this distribution appeared to provide a simple explanation for the so-called glass transition observed in proteins at 200 K (*22*). Here we focus on the details of the dynamics revealed by the temperature dependence of nitrogen-15 and deuterium relaxation in CaM complexed to the smMLCKp domain. To aid in the interpretation of the temperature dependence, we also examine the behavior of several simple physical models, including one that incorporates cooperative or coupled motion with neighboring side chains.

MATERIALS AND METHODS

Samples. Chicken calmodulin was expressed and purified as described previously (*23*). For the ^{2}H relaxation NMR sample, *Escherichia coli* BL21(DE3) cells were grown on minimal media containing 50% H_2O and 50% D_2O and using $^{15}NH_4Cl$ and D-glucose (U-$^{13}C_6$, 99%) as the sole nitrogen and carbon sources, respectively. For the ^{15}N relaxation sample, cells were grown on 100% H_2O minimal media containing $^{15}NH_4Cl$ and unlabeled glucose.

A peptide from the chicken smooth muscle myosin light chain kinase (smMLCKp, GSARRKWQKTGHAVRAIGRLS) was subcloned into a pET32 vector (Novagen Inc.) behind a T7 promoter as a thioredoxin fusion protein with a C-terminal His tag followed by the thrombin cleavage site and the smMLCKp sequence. This construct was transformed into *E. coli* BL21(DE3) cells and grown on rich media at 37 °C until an OD_{600} of 0.6−0.7 was reached, at which point isopropyl β-D-thiogalactopyranoside was added to 1 mM to induce overexpression of fusion protein. After 3 h of induction, cells were harvested and loaded onto a 10 mL Ni-NTA agarose column (Qiagen Inc.) equilibrated in binding buffer (20 mM Tris-HCl, pH 7.9, 0.5 M NaCl, 5 mM imidazole). The column of bound thioredoxin−smMLCKp fusion protein was washed with 60 mM imidazole, eluted with 0.5 M imidazole, and dialyzed into thrombin cleavage buffer (20 mM Tris-HCl, pH 8.4, 150 mM NaCl, 2.5 mM $CaCl_2$). The fusion protein was cleaved with ∼20 nM thrombin for approximately 2 h at room temperature in a 10−15 mL reaction volume. Cleavage products were stored at −20 °C until purification by high-pressure liquid chromatography using a C-8 reversed-phase column.

The CaM·smMLCKp complexes (for ^{15}N and ^{2}H relaxation samples) were formed by titrating ∼2 mM unlabeled peptide into 0.3 mM CaM in buffer conditions 4-fold dilute relative to the final NMR conditions of the intact complex. All titrations were monitored by HSQC spectra to confirm that the complex was in slow exchange on the NMR time scale and to ensure a CaM·smMLCKp stoichiometry of 1:1.0−1:1.1. The final solution conditions in 93%:7% H_2O:D_2O were 1.2 mM complex, 10−20 mM imidazole-d_4, pH 6.5, 100 mM KCl, 6 mM total $CaCl_2$, and 0.02% NaN_3. For the 50% randomly fractionally deuterated (and uniformly ^{13}C, ^{15}N enriched) CaM sample, deuterated bis-Tris (CIL Inc.) was substituted for imidazole.

NMR Spectroscopy. NMR data were collected using Varian Unity Inova spectrometers equipped with triple-resonance probes and *z*-axis pulsed-field gradients. All ^{15}N pulses were applied at 7.1 kHz, except for acquisition decoupling which was applied at 1−2 kHz. High-power and acquisition decoupling ^{13}C pulses were delivered at 20 and 2 kHz, respectively. High-power and decoupling ^{2}H pulses were delivered at 2.4 and 0.8 kHz, respectively. ^{15}N and ^{13}C pulses were found to be invariant with temperature, although ^{13}C pulse widths increased slightly at temperatures over 60 °C. For each temperature, on each spectrometer, temperature calibrations were made with methanol up to 35 °C and with ethylene glycol at higher temperatures.

^{15}N T_1, T_2, and {^{1}H}−^{15}N NOE experiments (*24*) were acquired with our normal modifications: two high- power, initial ^{1}H saturation pulses were inserted at the beginning of the T_1 relaxation delay (*25*); ^{1}H decoupling/saturation during

T_1 was accomplished with hard 120° pulses spaced every 5 ms; and the second half of the T_2 CPMG was removed to give a block duration of ~8 ms. The two experiments comprising the NOE were acquired in an interleaved fashion. T_1 and T_2 experiments were typically acquired with nine relaxation time points with three additional "duplicate" time points, which were used to assess peak intensity uncertainties. For T_1, relaxation curves were typically sampled out to 1.5−2 times the value of the expected T_1, and sample times were adjusted for each temperature. For T_2, relaxation curves were sampled out to ~120 ms; sampling of significantly longer times results in the onset of sample heating.

^{15}N relaxation data sets were collected at 11.7 T for 22, 35, 47, and 60 °C; the 73 °C data set was collected at 14.1 T. For all experiments, the ^{15}N carrier was placed at 118 ppm, and the indirect nitrogen acquisition times ranged from 85 to 100 ms; ^{15}N spectral widths were 31 ppm. ^{1}H acquisition times were typically 64 ms. For T_1 experiments, recycle delay times ranged from 1.3 s at 22 °C to 1.8 s at 73 °C, and 8−16 scans/fid were recorded. For T_2 experiments, recycle delay times were typically 1.5 s at the three lowest temperatures and 2.2 s at the two highest temperatures, and 8−16 scans/fid were recorded. For NOE experiments, ^{1}H irradiation was applied for 5.5, 4.5, 4.0, 4.0, and 4.0 s at 22−73 °C, respectively, yielding matched total recycle delay times in the corresponding reference experiments of 5.7, 5.0, 5.0, 5.0, and 5.0 s. These delay times were set to be 5−10 times the average ^{15}N T_1 value at each temperature.

^{2}H relaxation rates of side chain methyl CH_2D isotopomers were monitored using the trio of multiple coherence relaxation experiments of Kay and co-workers (*26*): I_zC_z, $I_zC_zD_z$, and $I_zC_zD_y$. These three experiments were carried out at 14.1 T at 15, 22, 28, 35, 38, 41, 44, 47, 50, 53, 60, 67, and 73 °C, for a total of 39 relaxation experiments over an 11 month period. The order of acquisition at various temperatures was shuffled in order to prevent irreversible changes in the sample being misinterpreted as a temperature dependence, although the experimental trio was always acquired sequentially in one session. Additional data sets were collected at 17.6 T at 15, 22, 35, and 47 °C; these extra data were necessary for reducing error bars of fitted model-free parameters at 15 and 22 °C, and at 35 and 47 °C the data at an additional field showed that obtained S^2_{axis} parameters were not dependent on the magnetic field strength at which the ^{2}H relaxation data were acquired. The ^{13}C carrier was placed at 18.1 ppm, and for the indirect ^{13}C dimension, the spectral width was 19.6 ppm, and 83 complex points were acquired (for 14.1 T). Typically, 16, 32, and 32 scans/fid were recorded for I_zC_z, $I_zC_zD_z$, and $I_zC_zD_y$. Typical recycle delays were 1.8−2.2 s. For each experiment, nine time points were collected with three duplicate points. For example, at 47 °C, relaxation delays were as follows (asterisks denoting duplicate measurements): I_zC_z at 12.1*, 22.3, 33.5, 44.7*, 55.9, 67.1, 78.3, 89.6*, and 101.1 ms; $I_zC_zD_z$ at 4.15*, 10.9, 19.6, 30.0*, 41.8, 54.8, 68.9, 84.1, and 100.4 ms; $I_zC_zD_y$ at 0.7, 2.1*, 3.8, 5.9*, 8.3, 10.9, 13.7, 16.8*, and 20.0 ms. The sampling of multispin coherence relaxation was adjusted for each temperature to ensure optimal curves for nonlinear least-squares fitting. The ^{2}H spin lock in $I_zC_zD_y$ was calibrated at ~1.1−1.2 kHz (at 14.1 T) and was restricted to durations shorter than 30 ms.

$^3J_{CC}$ and $^3J_{CN}$ coupling constant measurements for were carried out at 600 MHz using standard two-dimensional methods (*27*, *28*).

Relaxation Data Analysis. Relaxation decays from ^{15}N T_1, ^{15}N T_2, I_zC_z, $I_zC_zD_z$, and $I_zC_zD_y$ experiments were obtained from maximal peak intensities and fitted to single exponentials using two-parameter nonlinear least-squares routines (*29*). The $\{^1H\}-^{15}N$ NOE was calculated as the ratio of peak intensities, I^{NOE}/I^{ref}. Pure ^{2}H longitudinal and transverse relaxation rate constants were extracted as the difference of I_zC_z from $I_zC_zD_z$ and $I_zC_zD_y$ rate constants, respectively (*26*).

Both ^{15}N and ^{2}H relaxation data were fitted to the original Lipari−Szabo model-free parameters (*30*) using an in-house Fortran program (*29*, *31*). Error bars were estimated on the basis of 150 Monte Carlo simulations.

Analysis of ^{15}N relaxation was initiated at each temperature by characterization of overall tumbling. Residues were excluded from this process if their NOEs were less than 0.65 or if their T_1/T_2 ratios deviated significantly from the average T_1/T_2 ratio at a given temperature using the criterion of Tjandra et al. (*32*). The latter test is useful for identifying residues exhibiting additional line broadening due to chemical exchange processes on the microsecond to millisecond time scale. Using software (R2R1_diffusion) provided by Prof. Art Palmer, the T_1/T_2 ratios from the subset of residues remaining were used along with the structural coordinates [molecules "A" and "E" from the structure of Meador et al. (*33*); PDB code 1cdl] to fit an axially symmetric rotational diffusion tensor for the complex (*34*). Isotropic τ_m values were determined using the same subset of residues to perform a global grid search of τ_m, fitting O^2 and τ_e locally at each site for each trial τ_m value (*31*).

Analysis of ^{2}H relaxation data was carried out as described previously (*29*) and is only briefly recounted here. Pure ^{2}H relaxation rates (see above) from one or two field strengths (14.1 T, or 14.1 and 17.6 T) were fitted using the simple model-free spectral density employing an isotropic τ_m. It is worth noting that the effect of anisotropic rotational diffusion on ^{2}H relaxation should be damped in the case of methyl ^{2}H relaxation relative to amide ^{15}N relaxation; reorientation of the principal axis of the electric field gradient tensor resulting from rapid methyl rotation (or three-site jumping) averages the relaxation rates corresponding to the various orientations of the C−D vector relative to the principal diffusion tensor axis. $O_{axis}{}^2$ values were obtained subsequently by division by 0.111, which assumes tetrahedral methyl geometry (*30*).

Interpretative Models. In an attempt to provide physical insight into the basic features of the side chain and main chain dynamics revealed by the NMR relaxation studies described here, we evaluated the generalized order parameters arising from motion in several simple azimuthally symmetric potential well models where the energy depends only on the angle θ with respect to the symmetry axis. The generalized order parameter was calculated to high precision by numerical integration of the angular partition function of the model of interest followed by evaluation of the mean squared cosine angular correlation, which in turn defines the generalized order parameter (*30*):

$$O = {}^3/_2\langle\cos^2\theta\rangle - {}^1/_2$$

The potentials considered were an infinite square well (SQ)

of width θ_c, quadratic (U2), quartic (U4), sixth power (U6), and a stepped square well (ST) where $U = 0$ for $\theta < \theta_s$ and $U = U_s$ for $\theta > \theta_s$ elsewhere. The power law and square well potentials are described by a single parameter, the force constant K or the well width, respectively. The square well potential would correspond to the often used "free diffusion in a cone" model. The step potential has two parameters, the well width and step height, θ_s, and U_s, respectively.

In an effort to examine the effects of rotamer interconversion (i.e., barrier crossing) on the interpretation of order parameters obtained from methyl groups, a potential energy function of the form $U(\theta) = E_0 - E_1 \cos \theta - E_2 \cos 3\theta$, where θ is the involved torsion angle, was utilized in a manner similar to that described above for the simple effective potentials.

To investigate cooperative or correlated motion, four groups representing side chains arranged in a cluster restricted to a plane were examined. Each group i ($i = 1, ..., 4$) can undergo angular motion over a restricted range ($\pm 45°$) in a potential that consists of two components.

(i) One component is an intrinsic invariant potential U_i that depends only on that group's angle, θ_i. This potential provides a general restoring force exactly as in the simple potential models above. We chose a step potential (with $\theta_s = 30°$) since this provides the greatest dynamic range of S with T.

(ii) The other is a nearest-neighbor overlap potential. The interaction of each pair of neighbors i and j (where $i-j = 1-2, 2-3, 3-4$, or $4-1$) is given as an overlap penalty of U_{ij} if their angular displacement from each other is $(\theta_j - \theta_i) < \theta_{ij}$.

Precise numerical integration of the angular partition function was performed by systematic evaluation of the total energy for all combinations of the four angles. From the partition function the joint angular probability function $p(\theta_1, \theta_2, \theta_3, \theta_4)$ is obtained and thus the order parameters and any required average properties.

RESULTS

Temperature Range of Relaxation Experiments. The CaM·smMLCKp complex was examined over a range of temperatures from 15 to 73 °C. Methyl chemical shifts patterns are unchanged, indicating that the complex structure is stable across the full temperature range examined (Figure 1). Values of ΔH, ΔG, and ΔC_p obtained from calorimetric studies of a nearly identical complex (*35*) also predict that dissociation of the bound target domain will occur at well over 100 °C.

The picosecond to nanosecond dynamics of CaM in complex with smMLCKp were probed along the main chain and in methyl-bearing side chains, using ^{15}N and methyl ^{2}H relaxation methods, respectively. ^{15}N relaxation was monitored at five temperatures (22, 35, 47, 60, and 73 °C) using standard T_1, T_2, and $\{^1H\}-^{15}N$ NOE experiments (*24*) at either 11.7 or 14.1 T. ^{2}H methyl relaxation was monitored at 13 temperatures (15, 22, 28, 35, 38, 41, 44, 47, 50, 53, 60, 67, and 73 °C) using $^1H-^{13}C$ resolved ^{2}H relaxation experiments: I_zC_z, $I_zC_zD_z$, $I_zC_zD_y$ (see Materials and Methods). All ^{2}H relaxation data sets were collected at 14.1 T, although for a few temperatures additional sets were collected at 17.6 T. Data collected at two fields confirmed that obtained order parameters were not dependent upon the magnetic field

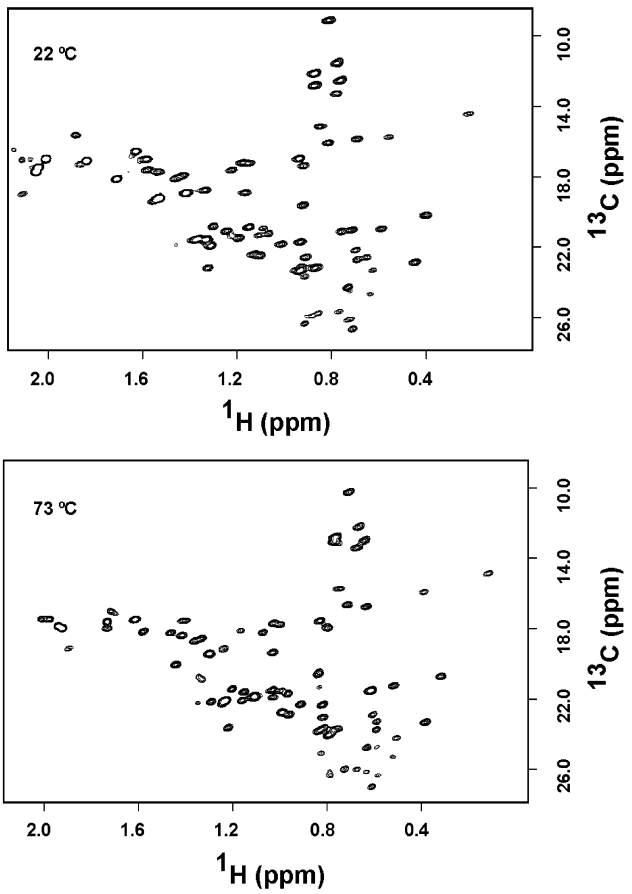

FIGURE 1: ^{13}C HSQC spectra of the calcium-saturated calmodulin−smMLCKp complex at 22 and 73 °C.

strengths used. All relaxation rates were interpreted within the model-free formalism, yielding a generalized order parameter describing restriction of motion, O^2, and an effective correlation time for the internal motion, τ_e (*30*). The relaxation data have been deposited in the BMRB under accession number 4970.

Determination of Correlation Times for Molecular Reorientation. To interpret relaxation data in terms of internal motion, the effects of overall tumbling must be factored out by determination of the overall correlation time, τ_m (*30*). This was accomplished in the standard manner (see Materials and Methods) at each of the five temperatures at which ^{15}N relaxation data were collected. We have previously reported evidence from multiple field relaxation measurements that ^{15}N T_1, T_2, and NOE data can have small but significant inconsistencies with respect to determination of τ_m; when T_2 is included in the model-free fits, τ_m becomes inflated by 5−10% relative to fits using only T_1 and NOE data (*36*, *37*). Because T_2 data are necessary for determining τ_m values longer than ~6 ns (*36*), T_2 had to be employed for most of the temperatures in the present study. Thus, for self-consistency across the temperature range, we have included T_2 data for all fits. However, to test the generality of the previous results, τ_m was determined using only T_1 and NOE data from 11.7 and 14.1 T at 73 °C. Whereas the τ_m determined using T_2 was 4.15 ns, the τ_m determined from T_1 and NOE data was 3.85 ns, approximately 7% shorter, consistent with previous observations. As expected, the isotropic τ_m values decrease as a function of increasing temperature (Figure 2a). Ideally, isotropic rotational diffusion

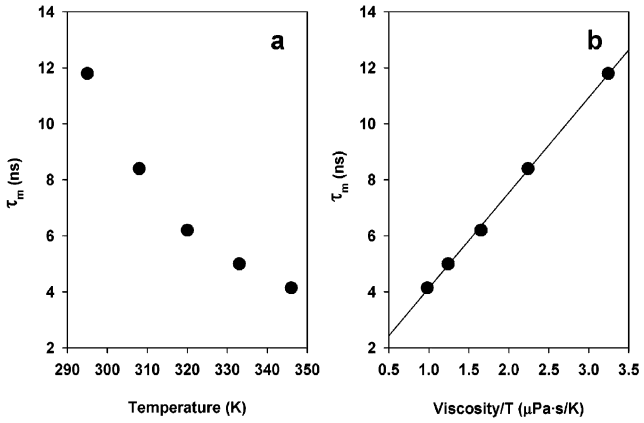

FIGURE 2: Characterization of molecular reorientation of the calcium-saturated calmodulin−smMLCKp complex. Isotropic molecular reorientation times were determined from analysis of ^{15}N relaxation data of backbone amide NH of calmodulin in the complex and are plotted against temperature (panel a) and against the ratio of the viscosity of pure water and the absolute temperature (panel b). The solid line in panel b is the best fit of the equation $\tau_m = a_0 + a_1(\eta/T)$.

should follow the Stokes−Einstein relation and vary linearly with respect to η/T. Under the assumption that the temperature dependence of the protein solution viscosity is proportional to the temperature dependence of the viscosity of H_2O, the rotational diffusion of the CaM·smMLCKp complex is well described by a simple linear relationship ($r^2 = 0.997$) (Figure 2b). The diffusion tensors from the four temperatures ranging from 22 to 60 °C are essentially identical; the average $D_\parallel/D_\perp$ is 1.12 ± 0.03 and average θ and ϕ values are 1.46 ± 0.13 and 2.95 ± 0.11 rad, respectively. At 73 °C, rotational diffusion becomes best described as "oblate" rather than "prolate"; $D_\parallel/D_\perp$ is 0.85 and θ and ϕ values are 1.21 and 1.37 rad. This result is simply due to the numerical ambiguity of the anisotropic tumbling equations under nearly isotropic tumbling conditions (*38*). Although the diffusion tensors at all five temperatures show small degrees of anisotropy ($0.8 < D_\parallel/D_\perp < 1.2$), this has very little effect on extracted O^2 values relative to use of an isotropic τ_m. Morever, use of the individually determined anisotropic diffusion tensors does not change the appearance of the order parameter temperature profiles nor does it alter any of the conclusions reached. For these reasons, isotropic rotational correlation times were used at all temperatures. The fitted temperature dependence was interpolated to obtain τ_m values for any temperature. The τ_m values used were 14.92 ns (15 °C), 11.81 ns (22 °C), 9.91 ns (28 °C), 8.26 ns (35 °C), 7.69 ns (38 °C), 7.19 ns (41 °C), 6.74 ns (44 °C), 6.33 ns (47 °C), 5.97 ns (50 °C), 5.64 ns (53 °C), 5.00 ns (60 °C), 4.47 ns (67 °C), and 4.10 ns (73 °C).

Temperature Dependence of Backbone Dynamics. Amide backbone dynamics were probed on the picosecond to nanosecond time scale at five temperatures, based on the analysis of ^{15}N T_1, T_2, and $\{^1H\}-^{15}N$ NOE experiments. Evidence for microsecond to millisecond time scale motion, indicated by a deviation of the field dependence of the T_2, was barely detectable at the lowest temperature (22 °C) and was completely absent above 47 °C. This general trend was also observed in the pioneering study of the temperature dependence of the backbone dynamics of ribonuclease H (*39*) and a C-terminal domain calmodulin mutant (*40*), although in the case of RNase H the effect was more pronounced than the present case. It should be noted that because the ^{15}N line broadening is small ($R_{ex} < 2$ s^{-1}), it is possible that the 19 T_2 values (out of 91) identified as containing R_{ex} contributions are shortened due to rotational anisotropy at 22 °C (*41*). Such a small degree of anisotropy, however, would not affect the extracted order parameters significantly, which is the main goal of the present study.

Overall, the majority of backbone amides are relatively rigid at low temperatures and exhibit a slight negative temperature dependence of their corresponding generalized order parameters; as the temperature is increased from 22 to 60 °C, O^2 values steadily decrease by $\sim -1.5 \times 10^{-3}$ K^{-1} on the average. Residues in helices have marginally larger temperature dependence than those in the short β sheets. For most amides, an apparent minimum in O^2 is observed at ~60 and is followed by a slight *rise* in order parameter at higher temperatures. This small but apparently significant positive temperature dependence in the 50−70 °C range is unexpected, and its physical origin is unclear. Various attempts were made to interpret this in terms of basic chemical parameters of the system. For example, use of a longer N−H bond length at 73 °C, possible from thermally excited vibrations, cannot explain the increase in O^2 since use of a longer bond length yields even higher order parameters. Increased H−D exchange rates can, in some situations, result in an underestimated (less negative) heteronuclear NOE that in turn results in a higher order parameter (*42*). In addition, use of an underestimated breadth of the amide nitrogen chemical shift tensor does result in a compensatory inflation of the fitted O^2 values for a given set of relaxation parameters [see Schneider et al. (*43*)]. Therefore, a temperature-dependent increase in the breadth of the amide nitrogen chemical shift tensor would result in an overestimation in fitted O^2 values with increasing temperature if a constant CSA tensor breadth is used, as is the case here. However, as outlined below, a physical (i.e., motional) mechanism could also give rise to this temperature dependence.

The dynamics of the amide NH of residues not involved in regular secondary structure have a relatively more variable temperature dependence (Figure 3). There are 24 residues in Ca^{2+}-binding loops (6 per EF hand) that are not in regular secondary structure, and there are 14 residues in loops that are neither in secondary structure nor in Ca^{2+}-binding loops. Some of the more mobile loop residues in the latter class could not be characterized at higher temperatures; for those amides not involved in hydrogen bonding, the increase in temperature severely reduced their peak intensities due to increased rates of ^{1}H exchange with solvent. Accordingly, much of the large-amplitude loop dynamics could not be followed, although in many cases dO^2/dT values could be obtained from two low-temperature points. On the average, loop residues involved with Ca^{2+} binding have order parameters ~0.05 lower than residues in helices or sheets. However, their temperature dependency as a group mirrors that of helices and sheets. Loop residues not involved with Ca^{2+} binding have the lowest backbone O^2 values, nearly 0.10 lower than residues in regular secondary structure. These residues as a group have the greatest temperature dependence, although this average feature is largely due to residues 115 and 116, which have dO^2/dT values of $\sim -5 \times 10^{-3}$ K^{-1}.

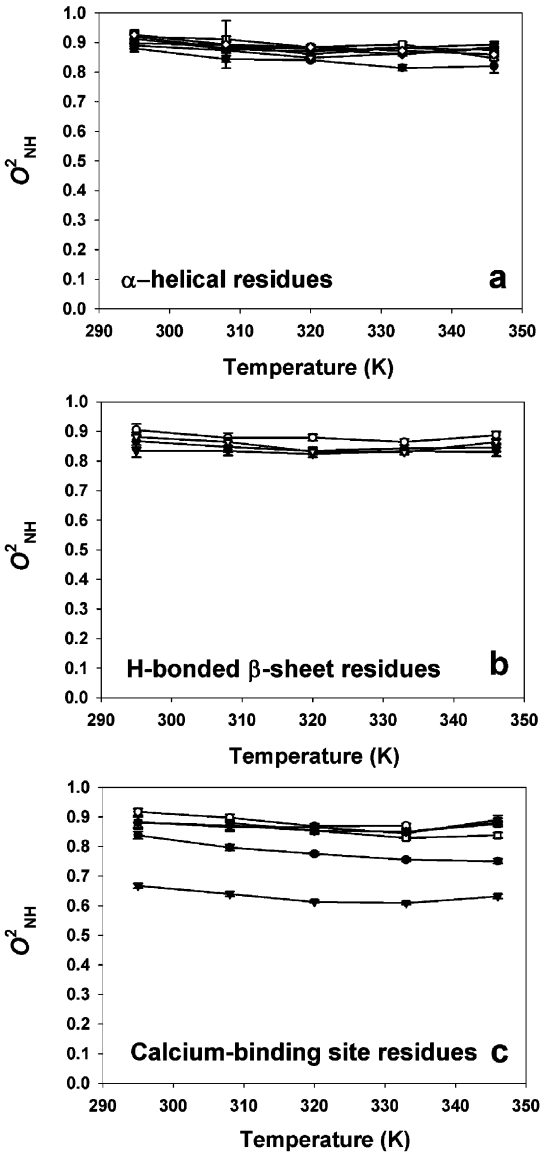

FIGURE 3: Temperature dependence of backbone amide O_{NH}^2 parameters obtained for calcium-saturated calmodulin in complex with the smMLCKp domain. Panel a shows representative examples of amide NH in α helices: Q8 (●), F16 (○), G33 (▼), T70 (▽), E87 (■), R106 (□), E123 (◆), and Q143 (◇). Panel b shows representative examples of hydrogen-bonded amide NH in β sheets: T27 (●), I63 (○), I100 (▼), and V136 (▽). Panel c shows representative examples of amide NH of residues in calcium-binding sites that are not involved in β sheet hydrogen bonding: K21 (●), T26 (○), A57 (▼), D64 (▽), N97 (■), D129 (□), and N137 (◆). In most cases, the error bars are less than the height of the symbols used.

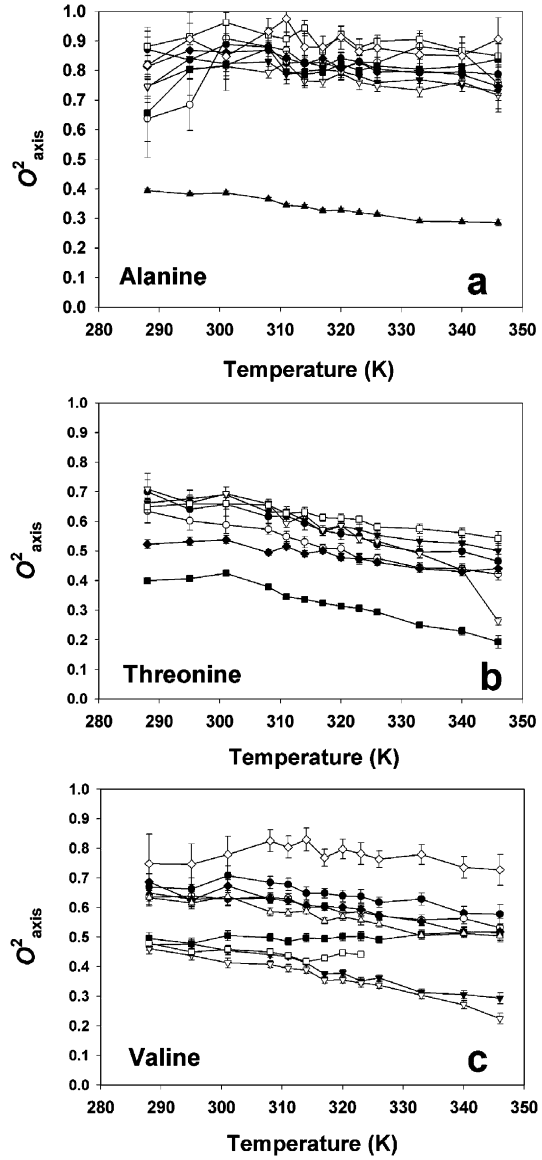

FIGURE 4: Temperature dependence of side chain methyl O_{axis}^2 parameters of calmodulin in complex with the smMLCKp peptide. Panel a, the methyl O_{axis}^2 parameters determined for the β-methyl groups of alanines: A10 (●), A15 (○), A46 (▼), A73 (▽), A88 (■), A102 (□), A103 (◆), A128 (◇), and A147 (▲). Panel b, the methyl O_{axis}^2 parameters determined for the γ-methyl groups of threonines: T26 (●), T29 (○), T34 (▼), T70 (▽), T79 (■), T110 (□), and T146 (◆). Panel c, the methyl O_{axis}^2 parameters determined for the γ-methyl groups of valines: V35-γR (●),V35-γS (○),V55-γR (▼),V55-γS (▽),V108-γR (■),V108-γS (□), and V121-γR (◆),-V136-γR (◇), V142-γR (▲), and V142-γS (△). In many cases the error bars are less than the height of the symbols used. See Figure 5 for similar data for isoleucine, leucine, and methionine residues.

The order parameters of residues 21 and 94 decrease by 0.09, with almost no curvature at the higher temperatures. Ala-57 also resides in position 2 of a Ca^{2+}-binding loop but has a lower O^2 of ∼0.65. It also has a temperature dependence more like the helical and sheet residues.

Methyl-Bearing Side Chain Dynamics. Methyl group dynamics were probed using ^{2}H-based relaxation methods (*26*). Longitudinal and transverse ^{2}H relaxation rates were monitored from $I_zC_zD_z$ and $I_zC_zD_y$ three-spin coherences, respectively; pure ^{2}H rates were obtained from subtraction of corresponding reference I_zC_z two-spin coherences (see Materials and Methods). The temperature profiles of methyl O_{axis}^2 parameters exhibit substantial variability in both absolute value and variation with temperature (Figure 4). A number of methyl groups display relatively large changes in order parameter at the temperature extrema (see Figure 4 and below). Discounting for the moment the data obtained at 15 and 73 °C, one can compare the average response of residue type to changes in temperature in the range of 22−67 °C (Table 1). On average, different methyl types have different temperature dependencies, (dO_{axis}^2/dT), or σ. A number of the alanine methyl groups display an apparent increase in the amplitude of their dynamics as the temperature falls below 28 °C (Figure 4). This is unexpected. Above 28 °C, the thermal response is roughly linear, having an average

Table 1: Thermal Coefficients of the Amplitude of Main Chain and Methyl-Bearing Side Chain Dynamics of Calcium-Saturated Calmodulin in Complex with the smMLCKp Domain[a]

	no.[b]	σ (K^{-1}) $\times 10^3$	r^2
amide N−H (O_{NH}^2)[c]	83	-1.5 ± 0.9	-0.89 ± 0.01
alanine βCH_3 (O_{axis}^2)[d]	9	-1.2 ± 1.2	-0.57 ± 0.40
	9	-1.7 ± 0.1	-0.66 ± 0.29[e]
threonine γCH_3 (O_{axis}^2)[d]	7	-3.9 ± 1.1	-0.97 ± 0.01
valine γCH_3 (O_{axis}^2)[d]	10	-1.8 ± 1.7	-0.47 ± 0.73
isoleucine γCH_3 (O_{axis}^2)[d]	6	-2.4 ± 1.2	-0.87 ± 0.19
isoleucine δCH_3 (O_{axis}^2)[d]	8	-2.4 ± 0.9	-0.82 ± 0.24
leucine δCH_3 (O_{axis}^2)[d]	7	-3.3 ± 1.3	-0.91 ± 0.07
methionine ϵCH_3 (O_{axis}^2)[d]	7	-3.8 ± 2.0	-0.97 ± 0.02

[a] Temperature coefficients dO^2/dT or σ for the indicated group are derived from linear regression of all data available, except as noted. The Pearson coefficient of correlation (r^2) and its standard deviation are shown to describe the degree of linearity of the response to temperature. [b] Number of sites for which reliable data at a minimum three temperatures was available. [c] Excluding the 73 °C data set; see text. [d] Excluding the 15 and 73 °C data sets; see text. [e] Excluding the 15, 20, and 73 °C data sets; see text.

σ of $\sim -1.8 \times 10^{-3}$ K^{-1}, similar to the backbone. It is interesting that the number of bonds a methyl group is removed from the backbone does not necessarily dictate the corresponding dO_{axis}^2/dT. For example, valine methyls have a relatively flat response to temperature with an average σ of $\sim -1.8 \times 10^{-3}$ K^{-1}. Furthermore, isoleucine γ- and δ-methyls have equivalent average thermal coefficients. Threonines have the largest σ of $\sim -3.9 \times 10^{-3}$ K^{-1}, although this may be a result of most of the threonines having high solvent accessibility in this protein complex. Methionines have the most variable and, interestingly, the most linear response to changes in temperature (Figure 4). The amplitudes of motion of some methionine methyl groups are relatively temperature insensitive (e.g., Met-76, $\sigma \sim -1.1 \times 10^{-3}$ K^{-1}) while others have among the largest thermal coefficients in the protein (e.g., Met-71, $\sigma \sim -6.3 \times 10^{-3}$ K^{-1}). In this vein, there would appear to be a rough correlation between the linearity of the temperature dependence of the amplitude of dynamics of a given amino acid side chain type, in the 28−67 °C range, and the number of bonds that the methyl group is from the backbone (Table 1).

The majority of methyl sites show a largely linear temperature dependence of O_{axis}^2 upon temperature. In contrast, the order parameters of some methyls decrease very little with temperature, and in the case of V108, the side chain apparently *loses* flexibility (i.e., increasing O_{axis}^2) with temperature. One group of methyls shows temperature profiles with a plateau in the 15−35 °C range (see Figures 4 and 5). These profiles exhibit a transition at ∼35 °C at which the O_{axis}^2 values begin to decline as the temperature is increased. This group is comprised mainly of β-branched residues, although β-branched residues are not restricted to this class. Another group of methyls have decreasing O_{axis}^2 values as the temperature decreases in the 15−30 °C range and thus exhibit a slightly "bowed" temperature profile. This group is dominated by isoleucine γ- and alanine β-methyls. Above 30 °C, the profiles are linear with temperature. Other apparent transitions in the amplitude of motion of some side chains are observed at the higher temperatures. For example, the initiation of a transition at 70 °C is clearly seen for $T70^{\gamma}$ as O_{axis}^2 values drop dramatically (Figure 4).

Intepretative Models of Motion. In an effort to gain insight into the physical origins of the observed dependence of main chain and side chain dynamics on temperature, we have carried out an analysis of motion under the influence of several simple potential energy functions. Four models were examined, all of which have azimuthally symmetric potential energy functions dependent upon a single geometric parameter. The temperature dependence of the generalized order parameter corresponding to motion under each potential energy function was numerically evaluated (see Materials and Methods). The infinite square well potential (SQ), which represents the often employed free diffusion in a cone model, was found, as is expected, to result in a temperature-*independent* order parameter (Figure 6). The other simple models show close to a linear decrease in O^2 with increasing temperature. Increasing the power of the *U*-type potentials decreases their *T* dependence, as they become more flat-bottomed, i.e., more square well-like (Figure 6). The step potential (ST), the most anharmonic of the simple models studied, gives the greatest temperature dependence, which is again close to linear. We also considered truncated, or flat-bottomed *U*-type potentials, to mimic a cage-like motion of a protein group through a small angular displacement. The results (not shown) are qualitatively similar to the corresponding nontruncated *U* potential but with a reduced temperature dependence.

Because the potential energy function defines the probability of occupancy of each potential state, the entropy of each model can be parametrically related to the corresponding generalized order parameter (*5*). This therefore provides experimental access to site-resolved information about protein residual entropy and, through its temperature dependence, the corresponding heat capacity. The relationship of the relative entropy for each model, obtained from the angular partition function by evaluating $\langle p(\theta) \ln p(\theta) \rangle$, to the corresponding order parameter is revealed by a variation of temperature (Figure 7). Interestingly, while the absolute value of entropy at a given value of order parameter varies between the different models, the curves are close to parallel. This characteristic was noted previously for the simple harmonic model (*5*) and proved to be extremely useful in the estimation of *changes* in conformational entropy involved in the association of calmodulin with a target domain (*44*). However, the large differences in absolute entropies across the various models indicate that it is much less reliable to estimate entropy changes if the character of the motion changes significantly in moving from one state to another. For example, in the unfolded state, a side chain or backbone element is likely to undergo a significantly different type of motion than when it is the compact folded state. Finally, except for the infinite square well potential, all of the potentials examined have a highly nonlinear dependence of the entropy at high values of O^2. This suggests that small changes of dynamics at relatively rigid sites can indeed correspond to large changes in entropy, emphasizing the need to consider backbone dynamics in detail.

The potentially large angular excursions of methyl groups having low generalized order parameters bring into consideration the possibility of barrier crossing from one rotomeric state to another. Motion involving barrier crossing would be qualitatively distinct from motion within a simple potential energy well. This type of motion is likely to contribute to

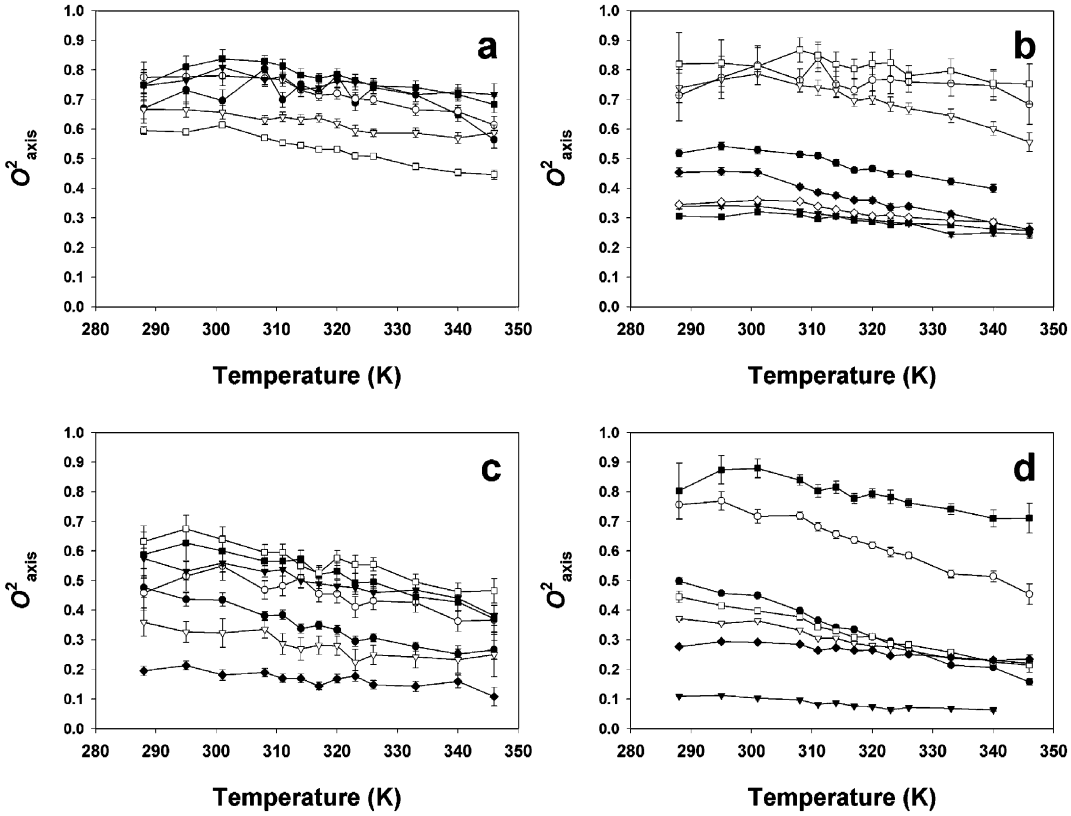

FIGURE 5: Temperature dependence of side chain methyl O_{axis}^2 parameters of calmodulin in complex with the smMLCKp peptide. Panel a, the methyl O_{axis}^2 parameters determined for isoleucine γ-methyls: I27 (●), I52 (○), I63 (▼), I85 (▽), I125 (■), and I130 (□). Panel b, the methyl O_{axis}^2 parameters determined for isoleucine δ-methyls: I9 (●), I27 (○), I52 (▼), I63 (▽), I85 (■), I100 (□), I125 (◆), and I130 (◇). Panel c, the methyl O_{axis}^2 parameters determined for leucine δ-methyls: L18δS (●), L39δR (○), L39δS (▼), L69δR (▽), L105δR (■), L112δS (□), and L116δR (◆). Panel d, the methyl O_{axis}^2 parameters determined for methionine δ-methyls: M71 (●), M72 (○), M76 (▼), M109 (▽), M124 (■), M144 (□), and M145 (◆). In many cases the error bars are less than the height of the symbols used. See Figure 4 for similar data for alanine, threonine, and valine residues.

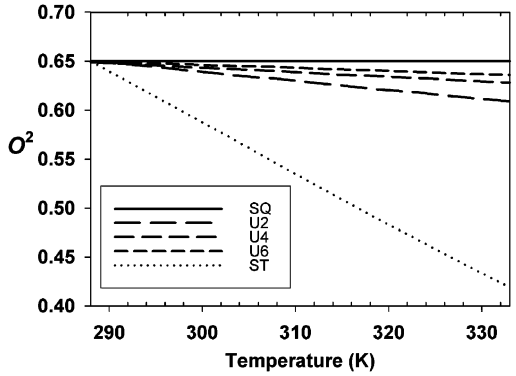

FIGURE 6: Temperature dependence of the O^2 parameter for a site moving in an infinite square well (SQ), quadratic (U2), quartic (U4), sixth power (U6), or stepped square well (ST) potential. The models have been parametrized to give an O^2 parameter value of 0.65 at a temperature of 15 °C.

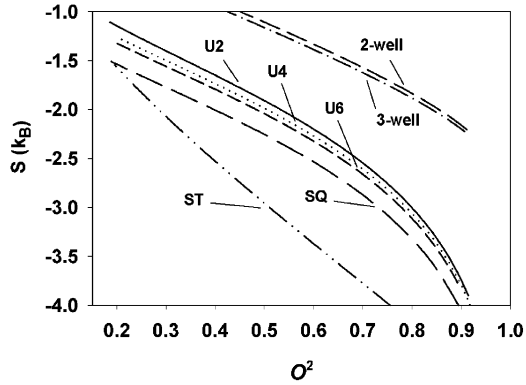

FIGURE 7: Parametric relationship between the O^2 parameter and corresponding relative entropy of a site moving in an infinite square well (SQ), quadratic (U2), quartic (U4), sixth power (U6), or stepped square well (ST) potential. Also shown is the parametric relationship for the two- and three-well model for rotomer interconversion (see Figure 8).

the high amplitude (lowest order parameter) class of motion. Indeed, a methyl group symmetry axis freely diffusing about a torsion angle within ±60° of its equilibrium position has a O_{axis}^2 of ~0.4. Larger amplitudes of motion would likely stray into the next rotomer "well". To further investigate the effects of such interconversion on obtained generalized order parameters, we have utilized the potential energy functions illustrated in Figure 8. Here we consider interconversion between three rotomers separated by 10−0 kT. Strictly speaking, the barrier separating the states should be low enough to allow interconversion on the time scale sensed by the relaxation methods employed here, i.e., on the subnanosecond time scale. This is required to satisfy the separation of time scales required by the Lipari−Szabo formalism and is supported by the obtained effective correlation times for motion of the symmetry axes. As illustrated in Figure 9, the generalized order parameter is reduced and the entropy increased by the presence of even small populations of minor rotomers.

Measurement of J coupling constants across involved χ_1 or χ_2 torsion angles failed to reveal the presence of extensive

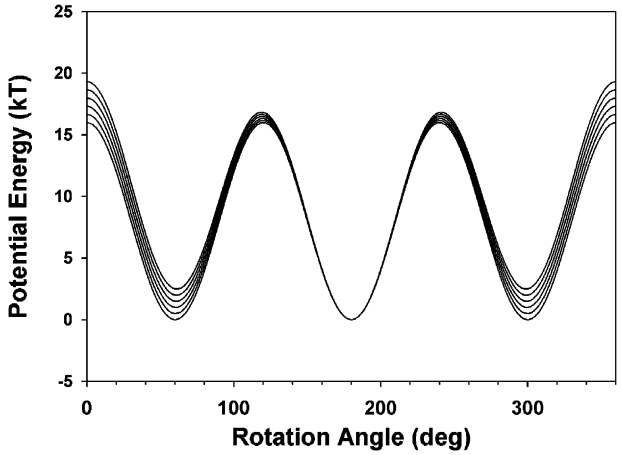

FIGURE 8: Potential energy functions used to simulate the effects of rotomer interconversion on generalized order parameters for attached methyl groups. The potential is defined by $U(\theta) = b_0 + b_1 \cos\theta + b_2 \cos 3\theta$. The constant b_1 was set to 8 kT. The constant $b_2 = \Delta U_{well}/1.5$ and $b_0 = b_1 + b_2$. ΔU_{well} was varied from 0 to 8 kT in steps of 0.5 kT to give the family of curves shown. This function defines three wells, two of which are degenerate. ΔU_{well} defines the energy gap between the two degenerate wells and the third well. The lowermost curve corresponds to ΔU_{well} of zero.

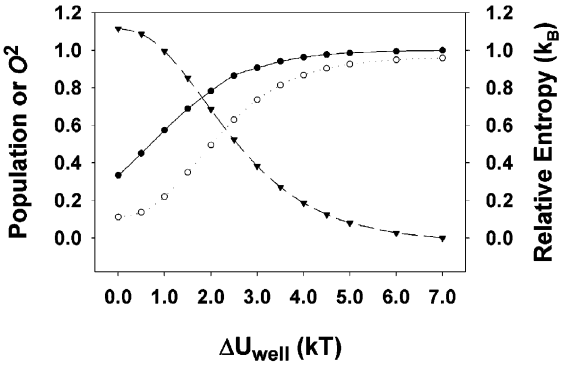

FIGURE 9: Dependence of the generalized order parameter and entropy on rotomer averaging. The curves were constructed using the potential energy function described in Figure 8 as a function of ΔU_{well}. Shown is the fractional occupancy of the major rotomer (●), the value of O^2 (○), and the difference in entropy from the high ΔU_{well} limit (▼).

averaging at either 25 or 60 °C (not shown). These results are similar to those obtained for free calcium-saturated calmodulin (*45*). However, exchange between a dominant rotomer and one or two minor rotomers (<10%) clearly might escape detection by this approach.

Effects of Conditional Motion. In an effort to illuminate the possible origins of various features of the observed temperature dependence of side chain motion in the calmodulin complex, we constructed a minimal model that could be treated exactly and capture the essential features of protein side chain motion in a tightly packed environment having extensive steric interactions and coupling with neighboring side chains. In short, this is used to represent a more general dynamically changing environment for a group rather than some invariant effective potential. This model is characterized by four intrinsic potential step barriers, Us_i, and four pairs of steric interaction parameters, $U_{ij}-\theta_{ij}$. Physically, the model can be thought of as describing the restricted range of angular motions intrinsic to each side chain because of covalent and backbone interactions, plus interactions with

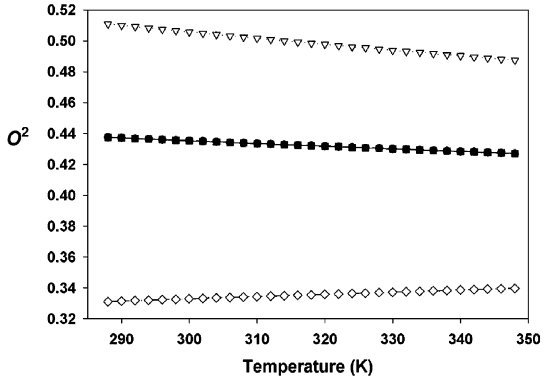

FIGURE 10: Temperature dependence of O^2 parameters of sites attached to the four interacting side chains of the cluster model. Side chains 1 and 3 have the same temperature dependence (○); side chain 2 (▼) and side chain 4 (▽) have negative and positive temperature dependencies, respectively.

neighboring side chains, where larger values of Us_i, U_{ij}, and θ_{ij} correspond respectively to a stiffer side chain, a harder neighbor interaction, and a looser packing with the neighbor, respectively.

A sterically interacting cluster model was examined in a variety of scenarios for side chain interaction, and the temperature dependence of the order parameters was obtained. The principle scenarios can be described as follows: (i) four noninteracting side chains (control); (ii) four equally stiff interacting side chains (symmetric case).

A series of nonsymmetric cases were obtained by systematic alteration of one parameter in case ii: (iii) one stiff side chain, three floppy side chains; (iv) one floppy side chain, three stiff side chains; (v) one loose neighbor interaction, three tight neighbor interactions; (vi) one tight neighbor interaction, three loose neighbor interactions; (vii) one hard neighbor interaction, three soft neighbor interactions; (viii) one soft neighbor interaction, three hard neighbor interactions; (ix) one stiff side chain ($Us_i = 1$ kcal) with loose neighbor interactions ($U_{ij} = 5$ kcal, $\theta_{ij} = 0$), three floppy side chains ($Us_i = 0$) making tight interactions with each other ($U_{ij} = 5$ kcal, $\theta_{ij} = 20$ for $i-j = 3-4$ and $4-1$).

Cases i−viii gave very similar results to the single group step potential model: monotonic, almost linear, decreasing O^2 with increasing temperature, with the expected variation among side chains, i.e., a higher O^2 for the stiffer side chain in case iii, the groups making the tight or hard interaction is cases vi, vii, etc. Case ix, corresponding to a more heterogeneous cluster interaction, gave a more interesting result (Figure 10). The central floppy side chain (4) shows an increase in O^2 with increasing T, while the stiff side chain (2) shows a decrease in O^2, and the intervening side chains (1 and 3) show almost no temperature dependence. The perhaps surprising increase in O^2 can be rationalized in physical terms as follows. Each side chain is constrained to move in some "configurationally averaged" space provided by its two neighbors. The side chain itself will tend to explore a larger volume, as the temperature is increased. However the "dynamic volume" occupied by its neighbors will tend also to increase as their excursions increase, sterically constraining the side chain. The net effect on the order parameter results from the competition between these two effects. In most scenarios, the first factor wins out, with the concomitant decrease in order parameter, since many of the

Table 2: Analysis of the Simple Cluster Model

Amplitude of Side Chain Motion				
side chain	1	2	3	4
$\sigma(\theta)$	22.926	20.101	22.926	32.026
Correlation Coeff between Side Chain Motions				
side chain	1	2	3	4
1	1.000	0.540	0.178	−0.508
2	0.540	1.000	0.540	−0.561
3	0.178	0.540	1.000	−0.508
4	−0.508	−0.561	−0.508	1.000

large excursions made by the neighbors are in the direction away from the side chain. Neighboring side chain motions tend to be positively correlated by their steric interaction. However, in case ix for the central floppy neighbor, the dynamic volume available to it is gradually decreased at higher temperatures because the stiff side chain opposite it starts to undergo larger excursions, "pushing" on the floppy intervening groups 1 and 3. This results in the increase in O^2 with temperature. In more formal terms, there is a negative correlation introduced between side chain 4's motion and side chain 2 (and, concomitantly, between 4 and 1/3) (Table 2). Case ix is the only one where negative angular correlation coefficients are seen between any side chains. It is also the only one where any *increase* in O^2 is seen. Finally, simulations of case ix indicate that the entropy of this cluster model is ~60% of that of the four side chains moving independently within their individual energy potentials.

Estimates of Protein Heat Capacity. Notwithstanding the issue of conditional motion, if we assume that the mean order parameter provides a good estimate of the net backbone entropy per residue, a range of 1.3−3.8 cal mol^{-1} K^{-1} residue^{-1} for the contribution of the backbone to the heat capacity of the folded protein is obtained using the relationship

$$C_p = \mathrm{d}S/(\mathrm{d}\ln T)$$

The mean methyl order parameter corresponds to an average from a range of side chain sizes, from small (Ala) to large (Met), and if these mean values are taken as representative of the motional order of all side chains, methyl and nonmethyl bearing, we estimate that the contribution to the protein heat capacity *reflected in the NMR order parameters* is in the range of 2.8−5.6 cal mol^{-1} K^{-1} residue^{-1}. These estimates of the protein heat capacity are significantly smaller than the estimates of 8 cal mol^{-1} K^{-1} residue^{-1} by Yang et al. (*46*) for an SH3 domain, largely because experimentally we have about the same change in O^2 over a much wider temperature range (51 versus 15 K). This reflects the fact that the calmodulin complex is much more stable. The lower end of the estimated range of protein heat capacity is also relatively small compared to the total system heat capacity typical of folded proteins with comparable stabilities (*47*, *48*). These and other results (*49*) are consistent with the view suggested by molecular dynamics simulations (e.g., ref *50*) that the majority of protein heat capacity arises from local bond vibrations, which are not directly sensed by the NMR measures used here.

DISCUSSION

The temperature dependence of the dynamics of the main chain is unremarkable in most respects. The backbone is largely highly ordered and relatively unresponsive to changes in temperature. The weak temperature dependence of O_{NH}^2 is largely linear except for an apparent upward inflection (decrease in amplitude) at many sites at the high end of the temperature range examined. In a density of states view, the smooth increase in amplitude of motion to a limiting value, before the subsequent reversal above 60 °C, may simply correspond to a saturation of the group of modes of motion available in this temperature range. The following decrease in amplitude of motion at higher temperatures has several potential explanations. It is possible that at elevated temperatures the rate of hydrogen exchange is sufficiently fast to contaminate the measurement of the heteronuclear NOE (*42*) and result in an artifactual increase in obtained generalized order parameters. Similarly, a systematic increase in the breadth of the CSA tensor with increasing temperature could result in an inflated fitted O_{NH}^2 using a temperature-independent and therefore underestimated CSA tensor breadth. A significant variation (10's of ppm) of the CSA tensor with temperature would be required to entirely explain deviation from a linear response to temperature. Information on the temperature dependence of amide nitrogen CSA tensors is sparse, but this magnitude of variation seems unlikely. Alternatively, as discussed below, the decrease in motional amplitude at elevated temperatures could also result from the steric coupling of motion of the amide N−H with neighboring groups.

The simple physical models used to explore the dependence of O^2 on temperature seem to show that no simple "effective potential" model is sufficient to explain the high temperature increase in $O_{NH}^2(T)$ or to capture the rich variety of observed $O_{axis}^2(T)$'s. Even though the step function potential has a relatively steep temperature dependence, it is, like all of the simple models, essentially linear and fails to show sharp transitions or reversals in sign. The failure of these simple models of motion in isolation is not too surprising since methyl groups are (usually) tightly packed in the protein and have covalent and steric interactions with neighboring groups which are themselves moving, presumably in a highly coupled way. This is also true for most amide NH. Thus the potential seen by a group is itself a dynamically changing factor. These conceptually intuitive features are represented in the simple cluster model. Simulations, particularly case ix, seem to suggest that the rich variety of $O_{axis}^2(T)$ behavior seen experimentally can, in principle, be explained only by including realistic features of the protein side chain interaction. Coupling of motion can result in suppression of thermal activation of motion at another site or even an increase in $O_{axis}^2(T)$ with increasing temperature.

A different type of complexity can arise through the superposition of motions (*30*, *51*). It is therefore interesting to note that the effective linearity of the response of the amplitude of motion to a change in temperature is most pronounced for the long side chains and less so for shorter side chains (see Table 1). Methionine methyls generally have the smoothest and most linear response to changes in temperature. This rough correlation would suggest that the presence of multiple modes (i.e., reorientation about multiple torsion angles) tends to smooth out the temperature response and, ironically, make it appear simpler. This type of model can, in principle, be directly tested by use of a recursive procedure, such as that used to analyze the dynamics of the

main chain of ubiquitin (*43*), to extract local contributions to a particular observed order parameter.

The physical origin of the three statistical groupings of the amplitudes of methyl-bearing side chain motion in proteins, first recognized in the calmodulin complex (*22*), remains somewhat of a mystery. It has been shown that proteins bearing large inflexible prosthetic groups such as heme (*52*) or flavin (*53*) can have the high amplitude motion of methyl-bearing amino acids essentially completely suppressed while in the other extreme a protein of de novo design that has otherwise nativelike properties shows complete absence of the lowest amplitude motional class (*37*). These few examples illustrate the variability of dynamical behavior available to proteins. In all cases thus far examined, however, the general grouping of dynamical amplitudes appears to be a common feature. It is this grouping of motional amplitudes that could provide a simple explanation for the abrupt change in temperature dependence at 200 K seen, for example, in inelastic neutron scattering profiles [e.g., Doster et al. (*54*)].

Two extreme situations can be imagined to give rise to discrete classes of motion. One is that the longer amino acid side chains can have three fundamental types of motion, each averaging the methyl symmetry axis to different degrees (*6*).[2] Motional averaging effects of this type have been suggested to influence obtained amide N−H generalized order parameters (*55*, *56*). Alternatively, one can imagine that there are truly three classes of distinct motional amplitudes. For example, as evidenced by Figure 9, variation of the barrier for rotomer interconversion from one residue to the next could easily introduce this behavior, and indeed, the very low generalized order parameters seen for one class of methyl-bearing side chains in the calmodulin complex would seem to require crossing from one rotomer to another. Obviously, further characterization utilizing additional probes on individual side chains is required (*6*).

Residual Protein Entropy and Heat Capacity. A very attractive feature of detailed, site-resolved information about internal protein dynamics is the potential of gaining access to the microscopic origins of residual protein entropy and derived quantities such as heat capacity. The use of site-resolved dynamics to provide an inventory of accessible states and hence act as a local "entropy meter" is fundamentally limited by an inability to detect and describe correlated motion. From the initial stages, it has been recognized that the simple site-resolved inventory of entropy ignores the very real possibility of correlated motion and the fact that single probes in a side chain need not sense all motions that are present. The latter difficulty can be dealt with by employing several probes throughout the side chain (*57*). Furthermore, the NMR-based measurements employed here are largely insensitive to the local motions arising from bond vibrations and hence are most useful in delineating the character of torsional oscillations about rotatable bonds.

The issue of correlated motion is somewhat resistant to direct resolution but has been suggested to be of modest concern (*58*). The four amino acid side chain cluster model utilized here allowed various aspects of cooperative or conditional motion by an amino acid side chain to be examined. Particularly noteworthy is the observation that the entropy of such clusters is not that different from the component side chains moving independently within their respective energy potentials. This raises significantly the confidence with which the use of parameters of local side chain dynamics can be used as measures of residual protein entropy contained in torsional oscillations, at least as reflected in the subnanosecond time scale motion between states.

[2] We gratefully acknowledge very fruitful discussion with Professor Erik Zuiderweg on this point.

ACKNOWLEDGMENT

We thank Dr. Peter Flynn for assistance with some of the relaxation experiments and Drs. Ad Bax, Dennis Torchia, and Erik Zuiderweg for helpful discussion.

REFERENCES

1. Doig, A. J. (1996) *Biophys. Chem. 61*, 131−141.
2. Pappu, R. V., Srinivasan, R., and Rose, G. D. (2000) *Proc. Natl. Acad. Sci. U.S.A. 97*, 12565−12570.
3. Shortle, D., and Ackerman, M. S. (2001) *Science 293*, 487−489.
4. Yang, D., and Kay, L. E. (1996) *J. Mol. Biol. 263*, 369−382.
5. Li, Z., Raychaudhuri, S., and Wand, A. J. (1996) *Protein Sci. 5*, 2647−2650.
6. Wand, A. J. (2001) *Nat. Struct. Biol. 8*, 926−931.
7. Pauling, L. (1948) *Nature 161*, 707−709.
8. Welch, G. R., Somogyi, B., and Damjanovich, S. (1982) *Prog. Biophys. Mol. Biol. 39*, 109−146.
9. Bruice, T. C., and Benkovic, S. J. (2000) *Biochemistry 39*, 6267−6274.
10. Rasmussen, B. F., Stock, A. M., Ringe, D., and Petsko, G. A. (1992) *Nature 357*, 423−424.
11. Kohen, A., Cannio, R., Bartolucci, S., and Klinman, J. P. (1999) *Nature 399*, 496−499.
12. Antoniou, D., and Schwartz, S. D. (2001) *J. Phys. Chem. B 105*, 5553−5558.
13. Balabin, I. A., and Onuchic, J. N. (2000) *Science 290*, 114−118.
14. Weber, G. (1975) *Adv. Protein Chem. 29*, 1−83.
15. Gurd, F. R. N., and Rothgeb, T. M. (1979) *Adv. Protein Chem. 33*, 73−165.
16. Englander, S. W., and Kallenbach, N. R. (1983) *Q. Rev. Biophys. 16*, 521−655.
17. Frauenfelder H., Parak F., and Young, RD. (1988) *Annu. Rev. Biophys. Biophys. Chem. 17*, 451−79.
18. Frauenfelder, H., Sligar, S. G., and Wolynes, P. G. (1991) *Science 254*, 1598−1603.
19. Wall, M. E., Ealick, S. E., and Gruner, S. M. (1997) *Proc. Natl. Acad. Sci. U.S.A. 94*, 6180−6184.
20. Palmer, A. G., III (1997) *Curr. Opin. Struct. Biol. 7*, 732−737.
21. Stone, M. F. (2001) *Acc. Chem. Res. 34*, 379−388.
22. Lee, A. L., and Wand, A. J. (2001) *Nature 411*, 501−504.
23. Urbauer, J. L., Short, J. H., Dow, L., and Wand, A. J. (1995) *Biochemistry 34*, 8099−8109.
24. Farrow, N. A., Muhandiram, R., Singer, A. U., Pascal, S. M., Kay, C. M., Gish, G., Shoelson, S. E., Pawson, T., Forman-Kay, J. D., and Kay, L. E. (1994) *Biochemistry 33*, 5984−6003.
25. Peng, J. W., and Wagner, G. (1994) *Methods Enzymol. 239*, 563−596.
26. Muhandiram, D. R., Yamazaki, T., Sykes, B. D., and Kay, L. E. (1995) *J. Am. Chem. Soc. 117*, 11536−11544.
27. Vuister, G. W., Wang, A. C., and Bax, A. (1993) *J. Am. Chem. Soc. 115*, 5334−5335.
28. Grzesiek, S., Vuister, G. W., and Bax, A. (1993) *J. Biomol. NMR 3*, 487−493.
29. Lee, A. L., Flynn, P. F., and Wand, A. J. (1999) *J. Am. Chem. Soc. 121*, 2891−2902.
30. Lipari, G., and Szabo, A. (1982) *J. Am. Chem. Soc. 104*, 4546−4559.
31. Dellwo, M. J., and Wand, A. J. (1989) *J. Am. Chem. Soc. 111*, 4571−4578.
32. Tjandra, N., Feller, S. E., Pastor, R. W., and Bax, A. (1995) *J. Am. Chem. Soc. 117*, 12562−12566.
33. Meador, W. E., Means, A. R., and Quiocho, F. A. (1992) *Science 257*, 1251−1255.

34. Lee, L. K., Rance, M., Chazin, W. J., and Palmer, A. G., III (1997) *J. Biomol. NMR 9*, 287−298.
35. Wintrode, P. L., and Privalov, P. L. (1997) *J. Mol. Biol. 266*, 1050−1062.
36. Lee, A. L., and Wand, A. J. (1999) *J. Biomol. NMR 13*, 101−112.
37. Walsh, S. T. R., Lee, A. L., DeGrado, W. F., and Wand, A. J. (2001) *Biochemistry 40*, 9560−9569.
38. Blackledge, M., Cordier, F., Dosset, P., and Marion, D. (1998) *J. Am. Chem. Soc. 120*, 4538−4539.
39. Mandel, A. M., Akke, M., and Palmer, A. G., III (1996) *Biochemistry 35*, 16009−16023.
40. Evenas, J., Forsen, S., Malmendal, A., and Akke, M. (1999) *J. Mol. Biol. 289*, 3−17.
41. Schurr, J. M., Babcock, H. P., and Fujimoto, B. S. (1994) *J. Magn. Reson, Ser. B 105*, 211−224.
42. Idiyatullin, D., Daragan, V. A., and Mayo, K. H. (2001) *J. Magn. Reson. 153*, 138−143.
43. Schneider, D. M., Dellwo, M. J., and Wand, A. J. (1992) *Biochemistry 31*, 3645−3652.
44. Lee, A. L., Kinnear, S. A., and Wand, A. J. (2000) *Nat. Struct. Biol. 7*, 72−77.
45. Chou, J. J., Li, S., Klee, C. B., and Bax, A. (2001) *Nat. Struct. Biol. 8*, 990−997.
46. Yang, D., Mok, Y., Forman-Kay, J., Farrow, N., and Kay, L. E. (1997) *J. Mol. Biol. 272*, 790−804.
47. Makhatadze, G., and Privalov, P. (1990) *J. Mol. Biol. 213*, 375−384.
48. Makhatadze, G., and Privalov, P. (1990) *J. Mol. Biol. 213*, 385−391.
49. Spracopoulos, L., Lavigne, P., Crump, M. P., Gagné, S., Kay, C. M., and Sykes, B. D. (2001) *Biochemistry 40*, 12541−12551.
50. Karplus, M., Ichiye, T., and Pettit, B. M. (1987) *Biophys. J. 52*, 1083−1085.
51. Wittebort, R. J., and Szabo, A. (1978) *J. Chem. Phys. 69*, 1722−1736.
52. Flynn, P. F., Flynn, P. F., Bieber Urbauer, R. J., Zhang, H., Lee, A. L., and Wand, A. J. (2001) *Biochemistry 40*, 6559−6569.
53. Liu, W., Flynn, P. F., Fuentes, E. F., Kranz, J. K., McCormick, M., and Wand, A. J. (2001) *Biochemistry 40*, 14744−14753.
54. Doster, W., Cusack, S., and Petry, W. (1989) *Nature 337*, 754−756.
55. Fischer, M. W., Zeng, L., Majumdar, A., and Zuiderweg, E. R. P. (1998) *Proc. Natl. Acad. Sci. U.S.A. 95*, 8016−8019.
56. Pang, Y., Buck, M., and Zuiderweg, E. R. P. (2002) *Biochemistry 41*, 2655−2666.
57. LeMaster, D., and Kushlan, D. (1996) *J. Am. Chem. Soc. 118*, 9255−9264.
58. Prompers, J. J., and Brüshweiler, R. (2000) *J. Phys. Chem. B 104*, 11416−11424.

BI026380D